Nanoparticles Self-Assembly Driven by High Affinity Repeat Protein Pairing

Kargal L. Gurunatha, Agathe C. Fournier, Agathe Urvoas, Marie Valerio-Lepiniec, Valérie Marchi, Philippe Minard, Erik Dujardin

Nanoparticles Self-Assembly Driven by High Affinity Repeat Protein Pairing

Kargal L. Gurunatha[1 †], Agathe C. Fournier[1], Agathe Urvoas[2], Marie Valerio-Lepiniec[2], Valérie Marchi,[3] Philippe Minard[2] and Erik Dujardin[1] **

[1] Groupe NanoSciences - CEMES-CNRS UPR 8011, 29 rue J. Marvig, B.P. 94347, F-31055 Toulouse, France.

[2] I2BC, Univ Paris Sud, CNRS, CEA UMR 9198, Bât. 430, F-91405 Orsay, France.

[3] University Rennes 1, Institut of Chemical Sciences, UMR 6226 CNRS, Campus Beaulieu, F-35042 Rennes France.

KEYWORDS. α-repeat proteins · gold nanoparticles · reversible self-assembly · protein pair · dissociation constant.

ABSTRACT. Proteins are the most specific yet versatile biological self-assembling agents with a rich chemistry. Yet, the design of new proteins with recognition capacities is still in its infancy and has seldom been exploited for the self-assembly of functional inorganic nanoparticles. Here, we report on the protein-directed assembly of gold nanoparticles using purpose-designed artificial repeat proteins having a rigid but modular 3D architecture. αRep protein pairs are selected for their high mutual affinity from a library of 10^9 variants. Their conjugation onto gold nanoparticles drives the massive colloidal assembly of free-standing, one-particle thick films. By lowering the average number of proteins per nanoparticle, the extent of self-assembly is limited to oligomeric particle clusters. Finally, we demonstrate that the aggregates are reversibly disassembled by an excess of one free protein. Our approach could be optimized for applications in biosensing, cell targeting or functional nanomaterials engineering.

Molecular self-assembly, specific recognition and reversible binding are ubiquitous mechanisms in living organisms where they underlie tissue growth and information processing, for instance. These mechanisms have inspired new concepts for the design and self -assembly of hybrid nanomaterials showing a wide range of innovative properties including sensing, data or energy storage and biocide activity.[1] In spite of tremendous progress in recent years, the challenge remains the control in time and space of the molecule-driven assembly sequences resulting in predictable and robust 3-dimensional organization of the nanosized building blocks.[2-4] Leading strategies have focused on refining the self-assembly, recognition and 3D topological organization capabilities of molecular scaffolds such as block copolymers,[5] amphiphilic peptide fibers,[6] solvent exclusion from hydrophobic polymer,[7] depletion in patchy nanoparticles[8, 9] or liquid crystals,[10] for example. Among promising mediators, biomolecules including DNA,[11-13] polypeptides [14, 15] and proteins [16-21] naturally fulfil most of the requirements. Directed self-assembly relies on two orthogonal approaches: templated self-assembly and direct partner recognition. The former consists in precisely positioning the nanoparticles with anchoring groups borne by a solid or supramolecular substrate. DNA origami templates,[22] peptides fibers,[23] β-sheets [24] or complex 3D architectures [25] and even 2D arrays of S-layer [26] and chaperonin proteins[27] as well as entire viruses (TMV,[28, 29] CCMV[30], CPMV[31]) have been successfully synthesized or modified to organize nanoparticles.[25] Yet template-mediated assembly fails to control the interparticle distance with the precision required for properties deriving from near-field coupling. In particular, the extreme sensitivity of the surface plasmon (SP) resonances to the spatial organization of the noble metal (*e. g.* Au, Ag) nanoparticles in close proximity to each other, has created a new ground for fundamental near-field optics,[32-35] quantum plasmonics,[36-38] enhanced spectroscopy and sensing applications, but imposes, in return, stringent conditions on

the precision of the interparticle distance.[39-42] In this respect, direct recognition produces colloidal aggregates with more precisely adjusted gap distances and hence improved collective properties. DNA hybridization between oligonucleotide strands tethered to Au nanoparticles was the first biomolecular implementation of direct coupling[43, 44] and has, so far, led to the most diverse approaches towards increased organizational and compositional complexity.[41, 45-48] Direct peptide coupling using coil-coil interactions [49, 50] has been exploited in a similar way.[51] Early attempts to demonstrate protein-driven self-assembly, after grafting the protein partners onto metallic nanoparticles, used the archetypal strong interaction between streptavidin and biotin.[52, 53] Other natural protein pairs have recently demonstrated the ability to precisely guide the 3D organization of colloids but the use of natural proteins is hampered by the absence of designability, which limits them to the discovered systems.[2, 54, 55] Antigen-antibody affinity pairs have also been considered early on and show the important assets of designability by standard phage display methods.[56] However antibodies are large molecules that are inefficiently produced as recombinant proteins in prokaryotic expression system because of their high propensity to aggregation, therefore limiting their use as self-assembly building blocks. A more promising approach is to mass produce recombinant proteins with a low aggregation propensity and a high folding efficiency.[18] Artificial proteins offer a unique way to interaction design and are creating opportunities to encode them with a highly versatile binding surface that can be optimized for improved specificity towards a chosen target. One class of appealing targets are proteins themselves in order to create high affinity protein pairs that serve as a generic and designable platform for the complex and specific self-assembly of functional colloids.[20]

In this Article, we report the massive assembly of Au nanoparticles driven by artificial repeat protein pairs. We demonstrate that α-repeat (αRep) protein pairs are a new class of self-

assembling agents able to organize functional colloids with a predefined specificity. The protein pairs are selected from a large library of 10^9 repeat proteins variants. The mutual affinity of the two biomolecular partners benefits from the highly stable periodic architecture and reaches nM dissociation constants. αRep have a common and rigid tertiary structure derived from the concatenation of a thermally stable α-helicoidal HEAT-like motif[18] and a variable surface corresponding to six hypervariable amino acid positions in each motif that do not affect the protein structure.[17, 57] As depicted schematically in **Figure 1**, the selected interactant proteins and the target are modified to create high affinity pairs that are grafted onto peptide-primed Au nanoparticles by the ligand exchange method. The mutual affinity of the grafted proteins induces the self-assembly of the gold nanoparticles as a first step towards new approach to rationally directed complex colloidal assembly with potential nano-optical applications.

Results and Discussion

The selection of protein pairs is carried out according to the method described in [57]. The combinatorial phage display technique is used to perform in-vitro directed evolution of the protein library in order to select individuals with high affinity (nM range) for a chosen αRep protein target, A3, the sequence of which comprises five variable repeats and is shown in **Figure 2**a(i). The cyclic process of selective enrichment and amplification leads to a pool of phages with potentially strong A3 binding ability. After three cycles, two different A3 binders, named α2 and α17, were selected and amplified. Although both proteins interact specifically with A3, they have different number of repeats (two and three respectively, excluding the C-cap) and different hypervariable sequences as can be seen from the sequences (ii) and (iii) in Figure 2a.

In order to graft the proteins onto the Au nanoparticles, a cysteine tag (CGCGCGS) is inserted at the C-terminal end. The αRep genes are sub-cloned into a new vector encoding the cysteine tag. The corresponding αRep-Cys_3 proteins are produced and purified under reducing conditions (1mM DTT) in order to avoid any disulphide bonds. In the case of tag-free A3•α2 complex, the X-ray crystallographic structure shows that the interaction occurs between the concave faces of the proteins, through four hydrogen bonds and three salt bridges.[57] The A3•α2 complex formation involves 19 residues of A3 and 22 residues of α2. The interacting residues of A3 originate from the N-cap (4 residues) and from the internal repeats (15 residues). All are found at hypervariable positions. The resolved structure of the A3•α2 complex (Figure 2b) suggests that the HEAT-repeat motif is preserved and that no steric hindrance in the complex mitigates with the protein backbone structure, which is globally preserved. The C-terminal Cys_3 tagging does not appear to modify the structure of the untagged protein pair nor the stability of the isolated or paired proteins.

A quantitative analysis of the binding affinity of α2-Cys_3 and α17-Cys_3 for A3-Cys_3 is obtained by isothermal titration calorimetry (ITC), which provides the dissociation constant, K_D, and complex stoichiometry, n.[57] The titrations of A3-Cys_3 by the Cys_3-tagged binders are shown in **Figure 3**. The K_D and n values are 4.2 ± 3.8 nM and 0.81 ± 0.01 for Cys_3-A3•α2-Cys_3 (Figure 3a) and 213 ± 25 nM and 0.86 ± 0.01 for Cys_3-A3•α17-Cys_3 (Figure 3b). Both complexes show a clear 1:1 stoichiometry alike the non-tagged proteins. However, the high affinity of α2-Cys_3 for A3-Cys_3 results in a very abrupt equivalence that makes it difficult to evaluate the dissociation constant. It can be re-evaluated by a competition experiment in which the Cys_3-A3•α17-Cys_3 complex is titrated with an excess α2-Cys_3. The heat-binding isotherm in Figure 3c shows a smooth transition that yield a dissociation constant of 12.9 ± 1.1 nM for Cys_3-

A3•α2-Cys_3. These experiments demonstrate that the nM affinity of the selected αRep protein pairs is only marginally affected by the cysteine tagging.[57]

Implementing steps I and II of the flowchart in Figure 1, the Cys-tagged proteins are grafted onto Au nanoparticles to drive the formation of higher order colloidal superstructures. In order to preserve the protein affinity intact once tethered to the metallic surface, the surface of the citrate-stabilized nanoparticles is first primed with a short anionic peptide ligand (C_3E_6Asp) composed of three functional blocks: a triple cysteine tag, that binds covalently to the gold surface, a 6-glycol spacer and an aspartate head group (pKa = 4.0) that bears a net negative charge at pH 7 (Step I). The large negative charge of the covalent capping layer provides an excellent colloidal stability, as can be inferred from the transmission electron micrographs (TEM) of the well-dispersed C_3E_6Asp-capped nanoparticles.[58] (**Figure 4a**). Moreover, no modification of the 520-nm surface plasmon resonance of the nanoparticles is observed after peptide capping (Figure 4e).

Next, the tagged αRep proteins are introduced in the capping layer by ligand exchange as detailed in the Supplementary Information (Step II).[59] The outcome of the protein insertion is monitored by stained TEM (Figure 4b-d) and UV-visible absorption (Figure 4e). Both techniques confirm that the colloidal suspensions of protein-functionalized nanoparticles remain stable, even 10 days after ligand exchange. In particular, no aggregation is observed.

TEM images of stained samples evidence the presence of a much thicker organic corona around the nanoparticles (insets of Figure 4b-d). This apparent thickness is commensurate with the protein size of ca. 5 nm and consistent with the estimated maximal stoichiometry of 4 proteins per nanoparticle, based on the respective molarity and sizes of nanoparticles and proteins, assuming a quantitative exchange probability. In order to assess the influence of the grafting stoichiometry, two nominal molar ratios of 20 or 30 proteins per nanoparticle are used.

The protein grafting does not change the general profile of the plasmon resonance band (Figure 4e). The marginal cumulated shift from 520 to 525 nm occurring during the Steps I and II is consistent with a small increase of the local refraction index upon replacing the citrate by the 5-nm thick peptide / proteins coating.

Figure 5a-c show the evolution of the electrophoretic properties of the Au nanoparticles on an agarose gel as they are primed with peptide and then functionalized with proteins. Citrate-stabilized Au nanoparticles bear a small net charge, consequently they do not migrate (Figure 5a, track 1). Once coated with C_3E_6Asp, the net negative charge per particles is significantly higher, which allows a significant and uniform migration (track 2). The grafting of the proteins affects the particle mobility differently depending on the balance between the increased hydrodynamic size and the net charge. The A3-functionalized nanoparticles migrates efficiently but show a large spread (track 3) whereas α2- and α17-functionalized nanoparticles migrate less but lead to narrower bands (tracks 4 and 5). Zeta potential measurements indicate that A3-functionalized nanoparticles bear a larger net charge at pH 7 than the ones derivatized with α2-Cys_3 or α17-Cys_3. This suggests that the attachment of the α2 and α17 proteins result in a significant conjugate size increase that is not compensated by a concomitant increase of net negative charge. Moreover, tracks 4 and 5 are narrow, which implies that the nanoparticles bear a similar number of proteins. On the contrary, the A3 : nanoparticle stoichiometry is less homogeneous, as revealed by the broader track 3, which could be in part due to the weak dimerization.[17] Interestingly, the colorimetric profiles of tracks 3-5 displayed in Figure 5b and 5c present a clear maximum at specific migration distance that can be used to identify the three types of bio-nano-conjugates.

The ability of artificial protein pairs to drive nanoparticle assembly (Step III in Figure 1) is investigated by mixing equimolar suspensions of A3-conjugated nanoparticles with either α2- or α17-conjugated nanoparticles (See Supplementary Information). The self-assembly is monitored by gel electrophoresis (GEP), UV-visible absorption (Figure 5) and TEM (**Figure 6**). The dielectrophoretic migration of both Au-A3•α2-Au and Au-A3•α17-Au duplex structures differs significantly from their isolated constituents (Figure 5, tracks 6 and 7). In particular, their respective colorimetric profiles 6 (Figure 5b) and 7 (Figure 5c) show maxima in between that of A3-Au and those of α2-Au or α17-Au respectively. The intermediate migration indicates that the A3-carrying nanoparticles are slowed down due to the drag of attached partner particles while the α2- and α17-carrying particles benefit from a better migration rate thanks to interaction with more charged species. These results strongly suggest that protein pair interaction takes place between Au nanoparticle populations. When a similar experiment is performed at lower nominal nanoparticle concentration, the bands of the assembled solutions can hardly be distinguished from the ones of isolated particles indicating a less effective pairing (See supplementary information, Figure S2). Importantly, all experiments are performed in BSA-primed containers to avoid protein adsorption on the plastic walls, following a well-established protocol for experiments involving specific protein interactions. Incidentally, the presence of adsorbed BSA also ensures that non-specific interactions are ruled out from the observed self-assembly.

The monitoring of the UV-visible spectra for 48 h after the mixing of the complementary nanoparticle populations produced with the high protein : nanoparticle molar ratio (30 : 1) shows a marked decrease of the SP resonance intensity but no spectral shift of the absorption maximum (Figure 5d curve 6 and Figure 5e curve 7). Moreover, minute amounts of thin black filaments are produced that settle rapidly. The absence of complete precipitation indicates that ill-controlled

aggregation by non-specific interactions does not occur. The decrease in absorbance for the Au-A3•α2-Au system is more important than for the Au-A3•α17-Au system, suggesting that a sizable fraction of the nanoparticles undergo self-assembly into large aggregates (filaments). Free particles that remain in suspension, due to the finite effective K_D, account for the subsistence of the unshifted SP band after mixing. It thus appears that the Au-A3•α17-Au is slightly less effective in driving large scale assembly in agreement with the higher K_D measured for the tagged protein pair A3•α17.

The superstructures obtained after self-assembly were examined in TEM. The morphology of the aggregates varies not only with the protein pairs but also with the grafting stoichiometry. Indeed the relative size of the nanoparticles and proteins, the protein-protein electrostatic repulsion as well as the kinetics of the ligand exchange reaction used for the surface immobilization limit the number of proteins per particle much below the geometrical limit of 20 proteins per 11-nm nanoparticle for A3, for example. If a majority of nanoparticles comprise more than 3 binding proteins, the assembly branches out isotropically into a 3-dimensional network. Conversely, if the stoichiometry is limited to 1 ; 1, nanoparticle dimers only will form. None of these extreme cases were observed in this work. Yet, when a high protein : nanoparticle molar ratio (30 : 1) was used to graft the biomolecules, the self-assembly of the resulting nanoparticle populations yields macroscopic filaments in a clear supernatant within 48 hours after mixing. SEM and TEM images of the filaments revealed massive micrometer-sized films composed of a uniform monolayer of densely packed nanoparticles (Figures 6a,b, S4 – S6). The general morphology of the monolayer film is similar with both proteins pairs but a slight difference in the average interparticle distance is observed. It is 3.5 ± 1.2 nm for Au-A3•α17-Au and 4.4 ± 1.2 nm for Au-A3•α2-Au (Figure S4). A very thin layer of protein is indeed visible

between the particles of the films, even without staining. Noteworthy, isolated nanoparticles or clusters are very seldom observed and the packing density of the nanoparticles is homogeneous throughout the film, which indicates that the monolayer film does not fragment or collapse upon deposition or drying. Neither spinodal drying patterns nor nanoparticle accumulation near the edge of the monolayer could be seen. Therefore, capillary artifacts due to drop-drying effects during sample preparation are unlikely to account for the monolayer formation. The observation of a free-standing film indicates that the protein : nanoparticle stoichiometry remains essentially between 1:1 and 3:1. In contrast, when the protein : nanoparticle molar ratio is reduced to 20 : 1, no extended monolayer films are found but finite-sized aggregates are produced with both protein pairs (Figures 6c and 6d). Flat clusters of a few tens of particles are seen with Au-A3•α17-Au (Figure 6c) while dimers, trimers and small chains of a few nanoparticles are observed with Au-A3•α2-Au (Figure 6d). A very thin layer of proteins along the nanoparticle chains is visible on magnified TEM images. Interestingly, the UV-visible spectral attenuation was not observed for conjugates produced with a nominal 20 : 1 molar ratio at the nanoparticle functionalization step (Fig. S3). In this case, the preservation of the plasmon resonance is attributed to the fact that finite size clusters remain suspended. No coupling between the individual bands occurs due to the large interparticle distance that exceeds 4-5 nm, whereas measurable red-shift is expected for sub-3 nm interparticle distance only (See simulations data in Fig. S3 and Fig. S6). We understand this change in superstructure morphology from film to clusters as the result of a variation of the amounts of mono-, di- and tri- topic conjugates, *i.e.* nanoparticles bearing 1, 2 or 3 binding proteins as detailed in Supplementary Information (Section 6). Indeed, the breadth of the bands in tracks 3 and 5 of Figure 5 suggests a range of stoichiometry for the high protein : nanoparticle molar ratio, but the corresponding bands in

tracks 3 and 5 in Figure S2 obtained for the low protein : nanoparticle molar ratio are both narrower and relatively closer to the injection well. This indicates that a smaller number of proteins attached, on average, on the nanoparticles when the protein : nanoparticle molar ratio is reduced. If tri-topic nanoparticles are present but significantly less frequent than ditopic ones, 3-dimensional networking is limited and the self-assembly proceeds in two dimensions resulting in monolayered film, as observed in Figures 6a,b but also for CdTe nanoparticles[60] and for DNA-linked metal nanoparticles,[61] for example. If the number of proteins available at the nanoparticle surface is further reduced, for example by reducing the protein concentration at the grafting stage, mostly di- and monotopic but few tri-topic conjugates are formed. The expansion of the self-assembly is limited by the more probable incorporation of mono-topic particles that stop the chain growth, thus quickly stopping the development of the aggregates. This results in finite sized clusters as illustrated in Figures 6c,d. In both cases, assembly is seen to proceed in two dimensions (film and flat clusters) rather than in disordered three dimensional networks and aggregates. We attribute this specific assembly morphology to the regular equatorial arrangement of the proteins on the nanoparticle surface as a result of the steric hindrance resulting between proteins grafted on a nanoparticle of similar size, of the inter-protein electrostatic repulsion. The rigid protein pair formation would preserve the directionality of particle-to-particle attachment in the film or clusters (See Section 5 in Supplementary Information).

Since the protein-directed self-assembly is governed by the association equilibrium of the protein duplex characterized by K_D, it can be reverted by adding one competing protein in large excess. In particular, the addition of a tenfold excess of the A3 protein bearing no cysteine tag to a conjugated Au-A3•α2-Au suspension triggers the entropic dissociation of the hybrid assembly to form Au-α2•A3 and concomitantly releases unbound Au-A3 in solution as schematized in

Figure 6e. Since all particles are primed with a peptide layer, the disconnected nanoparticles remain stable in suspension. When prepared in exactly the same conditions, the TEM samples of assembled Au-A3•α17-Au and Au-A3•α2-Au exposed to free A3 present isolated nanoparticles without any sign of massive or cluster aggregates as displayed in Figure 6f and 6g respectively. The disassembly is quite effective in spite of the presence of the proteins in the immediate vicinity of the particles as witnessed by the organic matrix surrounding the nanoparticles.

Conclusion

In conclusion, a family of artificial proteins with tailored binding affinity have been applied, for the first time, to the self-assembly of metallic colloids. This work demonstrates the concept that new pairs of proteins with high mutual affinity can be isolated, identified, mass-produced before they are attached to nanoparticles to drive their assembly. We have shown that the extent of the self-assembly process of protein-functionalized gold nanoparticles could be tuned between massive one-particle-thick films and finite sized nanoparticle clusters by changing the protein-particle stoichiometry. Moreover, exploiting the equilibrium properties of protein duplex formation, the aggregates have been reversibly disassembled into isolated nanoparticles. Since the protein pairs were identified by the highly combinatorial phage display approach, our concept opens the route to vast opportunities of optimization regarding the protein pair interaction properties, the protein-colloid chemistry and the reversibility mechanism. Finally, this work focuses on symmetrical gold-gold nanoparticle assembly. Yet, the αRep library is a generic source of specific proteins for arbitrary predefined biomolecular targets. For example, orthogonal protein pairs can be generated by this approach and grafted to other types of nanoparticles, thus

opening the way to an unlimited generalization to more complex functional assemblies. By combining the affinity and selectivity properties of proteins with the functionalities of inorganic nanoparticles, our approach pertains to a large number of application fields from (bio)sensing, cell targeting or functional nanomaterials design such as the reversible tuning of nano-optical properties.

Methods

Au nanoparticle synthesis. A 22 nM stable sol of monodispersed 11-nm diameter gold nanoparticles in water is synthesized by the classical reduction of tetrachloroauric acid by trisodium citrate.[62] The standard deviation of the nanoparticle diameter is about 10% from transmission electron microscopy analysis. The UV-visible spectrum of the citrate-stabilized Au nanoparticles shows a plasmon resonance centered at 520 nm. (See Section 2 in Supplementary Information)

Selection of interacting protein pairs by phage display. The selection of protein pairs has been carried out according to the method described in [57]. Briefly, a phage library displaying 10^9 variants of αRep proteins as fusion with the coat protein pIII is exposed to a target protein αRep A3, that comprises five variable repeats and a fixed C-cap (See sequence (i) in Figure 2a), for an affinity selection. The αRep library is assembled in a phage display phagemid vector.[17] Each bacterial cell produces phage particles with their associated αRep protein displayed on pIII . The variants of αRep proteins differ from each other by their sequence in hypervariable positions and / or by the number of repeat units. The affinity selection is performed on an immobilized target in Elisa plate. In the first selection round, phages showing affinity for the target A3 are captured when non-binding phages are washed away. The bound phages are then eluted and

amplified by infection in *E.coli* cells. Each bacterial cell produces phage particles with their associated αRep protein displayed on pIII. The amplified phage population is subjected to the next round of selection/amplification. After three rounds of selection, two different αRep binders named α2 and α17 are isolated and produced.

Peptide and protein conjugation on Au nanoparticles. A freshly prepared aqueous solution of *Cys-Cys-Cys-21-amino-4, 7, 10, 13, 16, 19-hexaoxaheneicosanoyl-aspartate* (C3E6Asp, 100 μL, 1 mM) in NaP 50 mM pH 7 buffer is added to 1 mL of the 22 nM Au nanoparticle suspension. The mixture is allowed to stand overnight at 12°C and under slow shaking at 400rpm to ensure a maximal covalent binding of the cysteine-tagged peptide.[58] Next, the peptide-stabilized nanoparticles are derivatized with αRep proteins. The intra and inter-protein disulfide bonds are reduced by incubation at 12°C for 2 hours in 100 mM DTT under slow stirring (400 rpm). The excess DTT is removed by elution through desalting column with NaP buffer (50 mM, pH 7). 3.6 μM activated protein solutions are collected. The Au nanoparticles are functionalized at the nominal molar ratio of 20 or 30 proteins per nanoparticle. For a 1:20 molar ratio, 150 μL of 3.6 μM protein solution is added very slowly to 1 mL of peptide-stabilized Au nanoparticles and left overnight at 4°C to allow ligand-exchange between the protein and the peptide. For the 1:30 molar ratio, the volume of 3.6 μM protein solution is 250 μL.

BSA priming of polystyrene containers. In order to reduce non-specific hydrophobic interaction of α-repeat proteins with the walls of Eppendorf tubes and 94-well plates, BSA is primed to the inner surface to reduce the protein loss during assembly experiments. 2% solution of BSA (50mM NaP buffer pH 7) is incubated in Eppendorf tubes or well plates for overnight and washed thoroughly with buffer solution and used in assembly experiment. Our previous

work on the protein pairs,[2] including crystallographic data, show that this priming method does not lead to BSA interference in the protein pair interaction.

Protein pair driven self-assembly. The protein-driven self-assembly experiments are run by mixing equimolar amount of A3-functionalized nanoparticles with α2- or α17-functionalized nanoparticles. In order to enhance the protein recognition, the starting nanoparticles suspension are concentrated five times by 11000 x g ultracentrifugation. Hence, 300 μL of 100 nM C3E6Asp-primed Au nanoparticles functionalized with A3 protein are mixed with 300 μL of 90 nM α2-functionalized Au nanoparticles. The mixture was incubated at 12°C for 1 hr and 400 rpm after which it is left undisturbed for 48 hr. The same procedure is used for a mixture of A3-functionalized Au nanoparticles and 90 nM α17-functionalized Au nanoparticles.

Affinity competition tests. Entropy-driven disassembly of the protein-pairs tethered to nanoparticles was tested by adding a 10-fold excess of αRep protein A3 bearing no Cys-tag. A minimum concentration of 10^{-5} M of αRep A3 (10 mL) in NaP 50mM pH7 buffer was introduced into the suspensions of assembled Au-A3•α2-Au or Au-A3•α17-Au and incubated at 12°C for 1 hr. A mild reduction of the color was noticed upon incubation. A control experiment on the possible effect of dilution was performed, where the free A3 protein aliquot was replaced by an identical volume of pure buffer did not yield to disassembly.

UV/Vis spectroscopic measurements. UV/Vis spectroscopic measurements were carried out using a Cary-5000 UV-Vis NIR spectrophotometer instrument operated by Carry UVWinLab (Version 1.1) software. Typical spectra were recorded in the range 200-800nm and at 600nm/min scan rate. A matched pair of Hellma QS 284 precision cells made of QUARTZ SUPRASIL (path length 1mm, working volume 250μL) was used to hold both the sample and reference solutions.

Transmission Electron Microscopy (TEM). TEM measurements of the samples were carried out on 300mesh carbon coated copper grids using PHILIPS CM20FEG or CM30 operating at 200kV or 150kV respectively accelerating voltage in bright field mode. The filament source is a Schottky field emission gun (FEG) or LaB6 (CM30). The microscope is equipped with a SC100 Orius CCD camera (11 megapixels) (FEG) or a CCD MSC 794 camera (CM30) mounted on 35mm port, which offers a large field of view. Microscope images were recorded on Gatan Digital Micrograph software.

TEM staining protocol: 1% of sodium phosphotungstate dibasic hydrate was prepared by dissolving metal salts in deionized water and then pH was adjusted to pH 7. The dried grid was taken and a drop of staining solution was added and left undisturbed for 3-5 min, washed once with distilled water and once dried, observed by TEM.

Agarose gel electrophoresis (GEP). To perform agarose gel electrophoresis of Au nanoparticles conjugated with peptide and protein, Enduro Gel XL with standard casting set, gel tank with safety lid and power supply, 120V (E0160) w/ FREE UPS was purchased from Labnet International Inc. For the preparation of the agarose gel: about 500mg of agarose was weighed and 100 mL of Tris borate 0.2 M buffer was added. The solution was heated at 85°C with stirring until all agarose dissolved in the buffer then the solution was slowly cooled down until 50°C and poured into gel tray. The comb was inserted and the solution was allowed to cool down for 30 min. It can be used by placing the gel in a buffer dam. Before running the samples, they were first mixed with 30% glycerol solution and then slowly injected in a well. A current of 100 mA is applied across the gel for 30 min.

Isothermal Titration Calorimetry (ITC). The binding parameters were monitored with an ITC 200 microcalorimeter (MicroCal). For the titration of target protein, 2 μL aliquots of the titrant

A3-Cys_3 (350 μM), were injected from a computer-controlled 40 μL microsyringe at intervals of 180 s into the solution of target (30 μM) in cell (volume 0.24 mL) dissolved in the same standard buffer (PBS) while stirring at 1000 rpm. The heat of dilution of the binder was determined from the peaks measured after full saturation of target by the binder. The data were integrated to generate curves in which the areas under the injection peaks were plotted against the ratio of injected sample to cell content. Analysis of the data is performed using the MicroCal Origin software provided by the manufacturer according to the one-binding-site model. ΔH°, the standard change in enthalpy and ΔG°, the standard change in Gibbs free energy, were calculated by integration of heat capacity variation from the titration curve and the associated equilibrium constant. ΔS°, the standard change in entropy upon binding, was calculated from determined equilibrium parameters using the equation: $-RTLn(K_A) = \Delta G° = \Delta H° - T\Delta S°$, where R is the universal gas constant (1.9872 $cal.mol^{-1}.K^{-1}$), T is the temperature in Kelvin, K_A is the association constant. The binding constant of each interaction is expressed as $1/K_A = K_D$ (in $mol.L^{-1}$), for more clarity.

The competition binding experiments corresponding to the displacement titration of a mixture of A3-Cys_3 (25 μM) in presence of α17-Cys_3 (45 μM) with α2-Cys_3 (350 μM) has been performed in the same standard buffer. Experimental data were fitted using the MicroCal Origin software according to the competitive binding model based on the analysis of competition ligand binding experiment by displacement.[63]

Zeta potential. The zeta potential measurements performed on Malvern Zetasizer at pH 7 of pure proteins are **-41.83 mV** for Cys_3-A3, **-29.6 mV** for Cys_3-α2 **and -40.9 mV** for Cys_3-α17. These are consistent with the protein pI, which are **5.43** for A3, **7.07** for α2 and **8.89** for α17. The measured zeta potential of pure Au nanoparticles **-24.3 mV** tend to decrease to **-19.1 mV**

when Cys_3-A3 protein was conjugated and a further decrease to **-18.2 mV** was observed with the conjugation of α-Rep-2cys and α-Rep-17cys proteins respectively.

ASSOCIATED CONTENT

Supporting Information. Materials; TEM and UV visible absorption spectrum of citrate-stabilized Au nanoparticles; Gel electro-phoresis of constituent and assembled protein-functionalized nanoparticles at low colloidal concentration; Scanning Electron Microscopy characterization of freestanding particle film assembled by protein pairing. This material is available free of charge *via* the Internet at http://pubs.acs.org.

AUTHOR INFORMATION

Corresponding Author

* Erik Dujardin, e-mail: dujardin@cemes.fr and Philippe Minard, e-mail: philippe.minard@u-psud.fr.

Present Addresses

† NanoEngineering Department, University of California San Diego, 9500 Gilman Drive MC 0448, La Jolla, California 92093, USA.

ACKNOWLEDGMENT

The authors thank S. Nessler for technical assistance. This work was funded by the European Research Council (ERC, Grant No FP7-ERC-2007-StG-203872 COMOSYEL to E. D.), a CNRS High Risk Program "NanoBriques" and by the Agence Nationale de la Recherche (ANR, Contract No ANR-14-CE08-0004-ARTEMIS).

Figure captions

Figure 1. Schematic flow chart of the Au NPs self-assembly driven by the αRep protein pair formation. Step I : anionic thiopeptide surface capping of citrate-stabilized Au nanoparticles. Step II : protein functionalization by ligand exchange. Step III : Nanoparticle self-assembly by protein pair recognition. Inset: TEM image of a massive nanoparticle film formed between A3- and α17-functionalized Au nanoparticles. Scale bar 2 μm.

Figure 2. (a) Amino acid sequence of the cysteine-tagged αReps (i) A3-Cys_3, (ii) α2-Cys_3 and (iii) α17-Cys_3. The Cys_3s tag is indicated in blue and the sequences also contain a N-terminal His6-tag (black). Green sections are the N-caps, red sections are the C-caps. Hypervariable positions are shown in orange . (b) Scheme of the interacting Cys_3-A3•α2-Cys_3 protein pair based on the crystallographic structure of the tag-free A3•α2 complex[57] placed between two schematic Au nanoparticle surfaces with schematic Cys_3 tags.

Figure 3. Micro-calorimetry (ITC) analysis of the A3-Cys_3-binding activity of (a) α2-Cys_3 (30 μM in cell) and (b) α17-Cys_3 (30 μM in cell). Experiments performed at 15°C in PBS (50 mM sodium phosphate pH 7, 150 mM NaCl) with 350 μM A3-Cys_3 in syringe. For each ITC experiment, the raw data (left panel) is integrated to obtain the saturation curve (right panel). (c) ITC analysis of the competition experiment between 350 μM α2-Cys_3 (in syringe) and 25 μM A3-Cys_3 pre-bound to 45 μM α17-Cys_3 (in cell).

Figure 4. TEM images of (a) Au NPs conjugated with a peptide and exchanged with b) A3cys_3, c) α2cys_3 and d) α17cys_3 proteins. The insets present the TEM images of the corresponding stained samples. (e) Normalized UV-visible spectra of the samples (a) to (d): in black the as-

synthesized Au NPs and in grey, the Au NPs functionalized with a peptide or an αRep protein (all data strictly overlap).

Figure 5. (a) Agarose gel electrophoresis of Au NPs stabilized by (1) citrate or (2) anionic C3E6Asp peptide. Tracks (3) to (5) correspond to Au NPs functionalized with αRep proteins A3-Cys_3, α2-Cys_3 and α17-Cys_3 respectively. The conjugates Au-A3•α2-Au and Au-A3•α17-Au are run in tracks (6) and (7) respectively. (b) Electrophoresis profile plots for tracks (3), (4) and (6) for the self-assembly driven by the A3•α2 pair. (c) Electrophoresis profile plots for tracks (3), (5) and (7) for the self-assembly driven by the A3•α17 pair. (d, e) UV-visible spectrophotometry of the corresponding experiments for (d) the A3•α2 pair and (e) the A3•α17 pair.

Figure 6. (a-d) TEM images of Au nanoparticles self-assembly induced by the affinity pairing of the conjugates A3•α17 (a, c) or A3•α2 (b, d) at a nanoparticle : protein molar ratio 1 : 30 (a : b) or 1 : 20 (c, d). (e) Schematic of affinity competition tests where the addition of a 10-fold excess of free αRep A3 bearing no cysteine tag induces the disassembly of the nanoparticle conjugates. (f, g) TEM images of the disassembled Au-A3• α2-Au (f) and Au-A3•α17-Au (g) conjugates after incubation in the presence of free A3.

REFERENCES

1. Nie, Z.; Petukhova, A.; Kumacheva, E. Properties and Emerging Applications of Self-Assembled Structures Made from Inorganic Nanoparticles. *Nat. Nanotechnol.* 2010, 5, 15-25.

2. Nikitin, M. P.; Zdobnova, T. A.; Lukash, S. V.; Stremovskiy, O. A.; Deyev, S. M. Protein-Assisted Self-Assembly of Multifunctional Nanoparticles. *Proc. Natl. Acad. Sci. U. S. A.* 2010, 107, 5827-5832.

3. Zhang, Y.; Lu, F.; Yager, K. G.; van der Lelie, D.; Gang, O. A General Strategy for the DNA-Mediated Self-Assembly of Functional Nanoparticles into Heterogeneous Systems. *Nat. Nanotechnol.* 2013, 8, 865-872.

4. Zhang, C.; Macfarlane, R. J.; Young, K. L.; Choi, C. H. J.; Hao, L.; Auyeung, E.; Liu, G.; Zhou, X.; Mirkin, C. A. A General Approach to DNA-Programmable Atom Equivalents. *Nat. Mater.* 2013, 12, 741-746.

5. Lopes, W. A.; Jaeger, H. M. Hierarchical Self-Assembly of Metal Nanostructures on Diblock Copolymer Scaffolds. *Nature* 2001, 414, 735-738.

6. Li, L. S.; Stupp, S. I. One-Dimensional Assembly of Lipophilic Inorganic Nanoparticles Templated by Peptide-Based Nanofibers with Binding Functionalities. *Angew. Chem., Int. Ed.* 2005, 44, 1833-1836.

7. Nie, Z.; Fava, D.; Kumacheva, E.; Zou, S.; Walker, G. C.; Rubinstein, M. Self-Assembly of Metal-Polymer Analogues of Amphiphilic Triblock Copolymers. *Nat. Mater.* 2007, 6, 609-614.

8. Wang, Y.; Wang, Y.; Breed, D. R.; Manoharan, V. N.; Feng, L.; Hollingsworth, A. D.; Weck, M.; Pine, D. J. Colloids with Valence and Specific Directional Bonding. *Nature* 2012, 491, 51-U61.

9. Desert, A.; Hubert, C.; Fu, Z.; Moulet, L.; Majimel, J.; Barboteau, P.; Thill, A.; Lansalot, M.; Bourgeat-Lami, E.; Duguet, E.; Ravaine, S. Synthesis and Site-Specific Functionalization of Tetravalent, Hexavalent, and Dodecavalent Silica Particles. *Angew. Chem., Int. Ed.* 2013, 52, 11068-11072.

10. Liu, Q.; Yuan, Y.; Smalyukh, I. I. Electrically and Optically Tunable Plasmonic Guest-Host Liquid Crystals with Long-Range Ordered Nanoparticles. *Nano Lett.* 2014, 14, 4071-4077.

11. Goodman, R. P.; Schaap, I. A. T.; Tardin, C. F.; Erben, C. M.; Berry, R. M.; Schmidt, C. F.; Turberfield, A. J. Rapid Chiral Assembly of Rigid DNA Building Blocks for Molecular Nanofabrication. *Science* 2005, 310, 1661-1665.

12. Nielsen, P. E.; Egholm, M.; Berg, R. H.; Buchardt, O. Sequence-Selective Recognition of DNA by Strand Displacement with a Thymine-Substituted Polyamide. *Science* 1991, 254, 1497-1500.

13. Seeman, N. C. DNA in a Material World. *Nature* 2003, 421, 427-431.

14. Mandal, D.; Shirazi, A. N.; Parang, K. Self-Assembly of Peptides to Nanostructures. *Org. Biomol. Chem.* 2014, 12, 3544-3561.

15. Wang, W.; Yang, Z.; Patanavanich, S.; Xu, B.; Chau, Y. Controlling Self-Assembly within Nanospace for Peptide Nanoparticle Fabrication. *Soft Matter* 2008, 4, 1617-1620.

16. Emberly, E. G.; Wingreen, N. S.; Tang, C. Designability of Alpha-Helical Proteins. *Proc. Natl. Acad. Sci. U. S. A.* 2002, 99, 11163-11168.

17. Urvoas, A.; Guellouz, A.; Valerio-Lepiniec, M.; Graille, M.; Durand, D.; Desravines, D. C.; van Tilbeurgh, H.; Desmadril, M.; Minard, P. Design, Production and Molecular Structure of a New Family of Artificial Alpha-Helicoidal Repeat Proteins (Alpha Rep) Based on Thermostable Heat-Like Repeats. *J. Mol. Biol.* 2010, 404, 307-327.

18. Boersma, Y. L.; Plueckthun, A. Darpins and Other Repeat Protein Scaffolds: Advances in Engineering and Applications. *Curr. Opin. Biotechnol.*2011, 22, 849-857.

19. Phillips, J. J.; Millership, C.; Main, E. R. G. Fibrous Nanostructures from the Self-Assembly of Designed Repeat Protein Modules. *Angew. Chem., Int. Ed.* 2012, 51, 13132-13135.

20. King, N. P.; Bale, J. B.; Sheffler, W.; McNamara, D. E.; Gonen, S.; Gonen, T.; Yeates, T. O.; Baker, D. Accurate Design of Co-Assembling Multi-Component Protein Nanomaterials. *Nature* 2014, 510, 103-+.

21. Mejias, S. H.; Sot, B.; Guantes, R.; Cortajarena, A. L. Controlled Nanometric Fibers of Self-Assembled Designed Protein Scaffolds. *Nanoscale* 2014, 6, 10982-10988.

22. Pal, S.; Deng, Z. T.; Wang, H. N.; Zou, S. L.; Liu, Y.; Yan, H. DNA Directed Self-Assembly of Anisotropic Plasmonic Nanostructures. *J. Am. Chem. Soc.* 2011, 133, 17606-17609.

23. Gottlieb, D.; Morin, S. A.; Jin, S.; Raines, R. T. Self-Assembled Collagen-Like Peptide Fibers as Templates for Metallic Nanowires. *J. Mater. Chem.* 2008, 18, 3865-3870.

24. Nonoyama, T.; Tanaka, M.; Inai, Y.; Higuchi, M.; Kinoshita, T. Ordered Nanopattern Arrangement of Gold Nanoparticles on Beta-Sheet Peptide Templates through Nucleobase Pairing. *ACS Nano* 2011, 5, 6174-6183.

25. Chen, C. L.; Zhang, P. J.; Rosi, N. L. A New Peptide-Based Method for the Design and Synthesis of Nanoparticle Superstructures: Construction of Highly Ordered Gold Nanoparticle Double Helices. *J. Am. Chem. Soc.* 2008, 130, 13555-+.

26. Hall, S. R.; Shenton, W.; Engelhardt, H.; Mann, S. Site-Specific Organization of Gold Nanoparticles by Biomolecular Templating. *ChemPhysChem* 2001, 2, 184-186.

27. McMillan, R. A.; Paavola, C. D.; Howard, J.; Chan, S. L.; Zaluzec, N. J.; Trent, J. D. Ordered Nanoparticle Arrays Formed on Engineered Chaperonin Protein Templates. *Nat. Mater.* 2002, 1, 247-252.

28. Bromley, K. M.; Patil, A. J.; Perriman, A. W.; Stubbs, G.; Mann, S. Preparation of High Quality Nanowires by Tobacco Mosaic Virus Templating of Gold Nanoparticles. *J. Mater. Chem.* 2008, 18, 4796-4801.

29. Dujardin, E.; Peet, C.; Stubbs, G.; Culver, J. N.; Mann, S. Organization of Metallic Nanoparticles Using Tobacco Mosaic Virus Templates. *Nano Lett.* 2003, 3, 413-417.

30. Aniagyei, S. E.; DuFort, C.; Kao, C. C.; Dragnea, B. Self-Assembly Approaches to Nanomaterial Encapsulation in Viral Protein Cages. *J. Mater. Chem.* 2008, 18, 3763-3774.

31. Blum, A. S.; Soto, C. M.; Wilson, C. D.; Brower, T. L.; Pollack, S. K.; Schull, T. L.; Chatterji, A.; Lin, T. W.; Johnson, J. E.; Amsinck, C.; Franzon, P.; Shashidhar, R.; Ratna, B. R. An Engineered Virus as a Scaffold for Three-Dimensional Self-Assembly on the Nanoscale. *Small* 2005, 1, 702-706.

32. Lin, S.; Li, M.; Dujardin, E.; Girard, C.; Mann, S. One-Dimensional Plasmon Coupling by Facile Self-Assembly of Gold Nanoparticles into Branched Chain Networks. *Adv. Mater.* 2005, 17, 2553-2559.

33. Jain, P. K.; Huang, W.; El-Sayed, M. A. On the Universal Scaling Behavior of the Distance Decay of Plasmon Coupling in Metal Nanoparticle Pairs: A Plasmon Ruler Equation. *Nano Lett.* 2007, 7, 2080-2088.

34. Kawata, S.; Inouye, Y.; Verma, P. Plasmonics for near-Field Nano-Imaging and Superlensing. *Nat. Photonics* 2009, 3, 388-394.

35. Dujardin, E.; Girard, C. Plasmonic Nanoparticle Networks. In *Handbook of Nanophysics* Sattler, K., Ed. Taylor & Francis: London, 2010; Vol. 3.

36. Marinica, D. C.; Kazansky, A. K.; Nordlander, P.; Aizpurua, J.; Borisov, A. G. Quantum Plasmonics: Nonlinear Effects in the Field Enhancement of a Plasmonic Nanoparticle Dimer. *Nano Lett.* 2012, 12, 1333-1339.

37. Scholl, J. A.; Garcia-Etxarri, A.; Koh, A. L.; Dionne, J. A. Observation of Quantum Tunneling between Two Plasmonic Nanoparticles. *Nano Lett.* 2013, 13, 564-569.

38. Tan, S. F.; Wu, L.; Yang, J. K. W.; Bai, P.; Bosman, M.; Nijhuis, C. A. Quantum Plasmon Resonances Controlled by Molecular Tunnel Junctions. *Science* 2014, 343, 1496-1499.

39. Eustis, S.; El-Sayed, M. A. Why Gold Nanoparticles Are More Precious Than Pretty Gold: Noble Metal Surface Plasmon Resonance and Its Enhancement of the Radiative and Nonradiative Properties of Nanocrystals of Different Shapes. *Chem. Soc. Rev.* 2006, 35, 209-217.

40. Shaw, C. P.; Fernig, D. G.; Levy, R. Gold Nanoparticles as Advanced Building Blocks for Nanoscale Self-Assembled Systems. *J. Mater. Chem.* 2011, 21, 12181-12187.

41. Liu, N.; Hentschel, M.; Weiss, T.; Alivisatos, A. P.; Giessen, H. Three-Dimensional Plasmon Rulers. *Science* 2011, 332, 1407-1410.

42. Hill, R. T.; Mock, J. J.; Hucknall, A.; Wolter, S. D.; Jokerst, N. M.; Smith, D. R.; Chilkoti, A. Plasmon Ruler with Angstrom Length Resolution. *ACS Nano* 2012, 6, 9237-9246.

43. Mirkin, C. A.; Letsinger, R. L.; Mucic, R. C.; Storhoff, J. J. A DNA-Based Method for Rationally Assembling Nanoparticles into Macroscopic Materials. *Nature* 1996, 382, 607-609.

44. Alivisatos, A. P.; Johnsson, K. P.; Peng, X. G.; Wilson, T. E.; Loweth, C. J.; Bruchez, M. P.; Schultz, P. G. Organization of 'Nanocrystal Molecules' Using DNA. *Nature* 1996, 382, 609-611.

45. Niemeyer, C. M.; Burger, W.; Peplies, J. Covalent DNA - Streptavidin Conjugates as Building Blocks for Novel Biometallic Nanostructures. *Angew. Chem., Int. Ed.* 1998, 37, 2265-2268.

46. Sadasivan, S.; Dujardin, E.; Li, M.; Johnson, C. J.; Mann, S. DNA-Driven Assembly of Mesoporous Silica/Gold Satellite Nanostructures. *Small* 2005, 1, 103-106.

47. Maye, M. M.; Nykypanchuk, D.; Cuisinier, M.; van der Lelie, D.; Gang, O. Stepwise Surface Encoding for High-Throughput Assembly of Nanoclusters. *Nat. Mater.* 2009, 8, 388-391.

48. Lu, F.; Yager, K. G.; Zhang, Y.; Xin, H.; Gang, O. Superlattices Assembled through Shape-Induced Directional Binding. *Nat. Commun.* 2015, 6, 6912-6912.

49. Papapostolou, D.; Smith, A. M.; Atkins, E. D. T.; Oliver, S. J.; Ryadnov, M. G.; Serpell, L. C.; Woolfson, D. N. Engineering Nanoscale Order into a Designed Protein Fiber. *Proc. Natl. Acad. Sci. U. S. A.* 2007, 104, 10853-10858.

50. Aili, D.; Gryko, P.; Sepulveda, B.; Dick, J. A. G.; Kirby, N.; Heenan, R.; Baltzer, L.; Liedberg, B.; Ryan, M. P.; Stevens, M. M. Polypeptide Folding-Mediated Tuning of the Optical and Structural Properties of Gold Nanoparticle Assemblies. *Nano Lett.* 2011, 11, 5564-5573.

51. Wagner, S. C.; Roskamp, M.; Coelfen, H.; Boettcher, C.; Schlecht, S.; Koksch, B. Switchable Electrostatic Interactions between Gold Nanoparticles and Coiled Coil Peptides Direct Colloid Assembly. *Org. Biomol. Chem.* 2009, 7, 46-51.

52. Connolly, S.; Fitzmaurice, D. Programmed Assembly of Gold Nanocrystals in Aqueous Solution. *Adv. Mater.* 1999, 11, 1202-1205.

53. Caswell, K. K.; Wilson, J. N.; Bunz, U. H. F.; Murphy, C. J. Preferential End-to-End Assembly of Gold Nanorods by Biotin-Streptavidin Connectors. *J. Am. Chem. Soc.* 2003, 125, 13914-13915.

54. Hiddessen, A. L.; Rodgers, S. D.; Weitz, D. A.; Hammer, D. A. Assembly of Binary Colloidal Structures *Via* Specific Biological Adhesion. *Langmuir* 2000, 16, 9744-9753.

55. Aghayeva, U. F.; Nikitin, M. P.; Lukash, S. V.; Deyev, S. M. Denaturation-Resistant Bifunctional Colloidal Superstructures Assembled *Via* the Proteinaceous Barnase-Barstar Interface. *ACS Nano* 2013, 7, 950-961.

56. Shenton, W.; Davis, S. A.; Mann, S. Directed Self-Assembly of Nanoparticles into Macroscopic Materials Using Antibody-Antigen Recognition. *Adv. Mater.* 1999, 11, 449-+.

57. Guellouz, A.; Valerio-Lepiniec, M.; Urvoas, A.; Chevrel, A.; Graille, M.; Fourati-Kammoun, Z.; Desmadril, M.; van Tilbeurgh, H.; Minard, P. Selection of Specific Protein Binders for Pre-Defined Targets from an Optimized Library of Artificial Helicoidal Repeat Proteins (Alpharep). *Plos One* 2013, 8, e71512.

58. Hamon, C.; Bizien, T.; Artzner, F.; Even-Hernandez, P.; Marchi, V. Replacement of Ctab with Peptidic Ligands at the Surface of Gold Nanorods and Their Self-Assembling Properties. *J. Colloid Interface Sci.* 2014, 424, 90-97.

59. Dif, A.; Boulmedais, F.; Pinot, M.; Roullier, V.; Baudy-Floc'h, M.; Coquelle, F. M.; Clarke, S.; Neveu, P.; Vignaux, F.; Le Borgne, R.; Dahan, M.; Gueroui, Z.; Marchi-Artzner, V. Small and Stable Peptidic Pegylated Quantum Dots to Target Polyhistidine-Tagged Proteins with Controlled Stoichiometry. *J. Am. Chem. Soc.* 2009, 131, 14738-14746.

60. Tang, Z.; Zhang, Z.; Wang, Y.; Glotzer, S. C.; Kotov, N. A. Self-Assembly of Cdte Nanocrystals into Free-Floating Sheets. *Science* 2006, 314, 274-278.

61. Cheng, W.; Campolongo, M. J.; Cha, J. J.; Tan, S. J.; Umbach, C. C.; Muller, D. A.; Luo, D. Free-Standing Nanoparticle Superlattice Sheets Controlled by DNA. *Nat. Mater.* 2009, 8, 519-525.

62. Frens, G. Controlled Nucleation for Regulation of Particle-Size in Monodisperse Gold Suspensions. *Nature, Phys. Sci.* 1973, 241, 20-22.

63. Sigurskjold, B. W. Exact Analysis of Competition Ligand Binding by Displacement Isothermal Titration Calorimetry. *Anal. Biochem.* 2000, 277, 260-266.

Table of Contents graphics

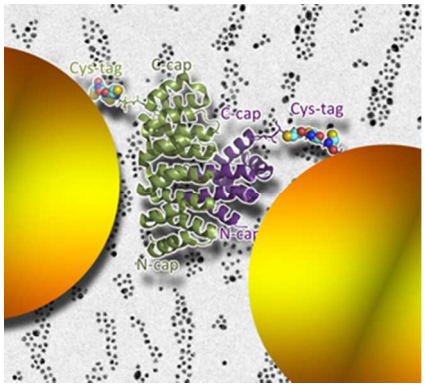

Purpose-designed, artificial repeat proteins with a modular and rigid 3D architecture are used to drive colloidal self-assembly.

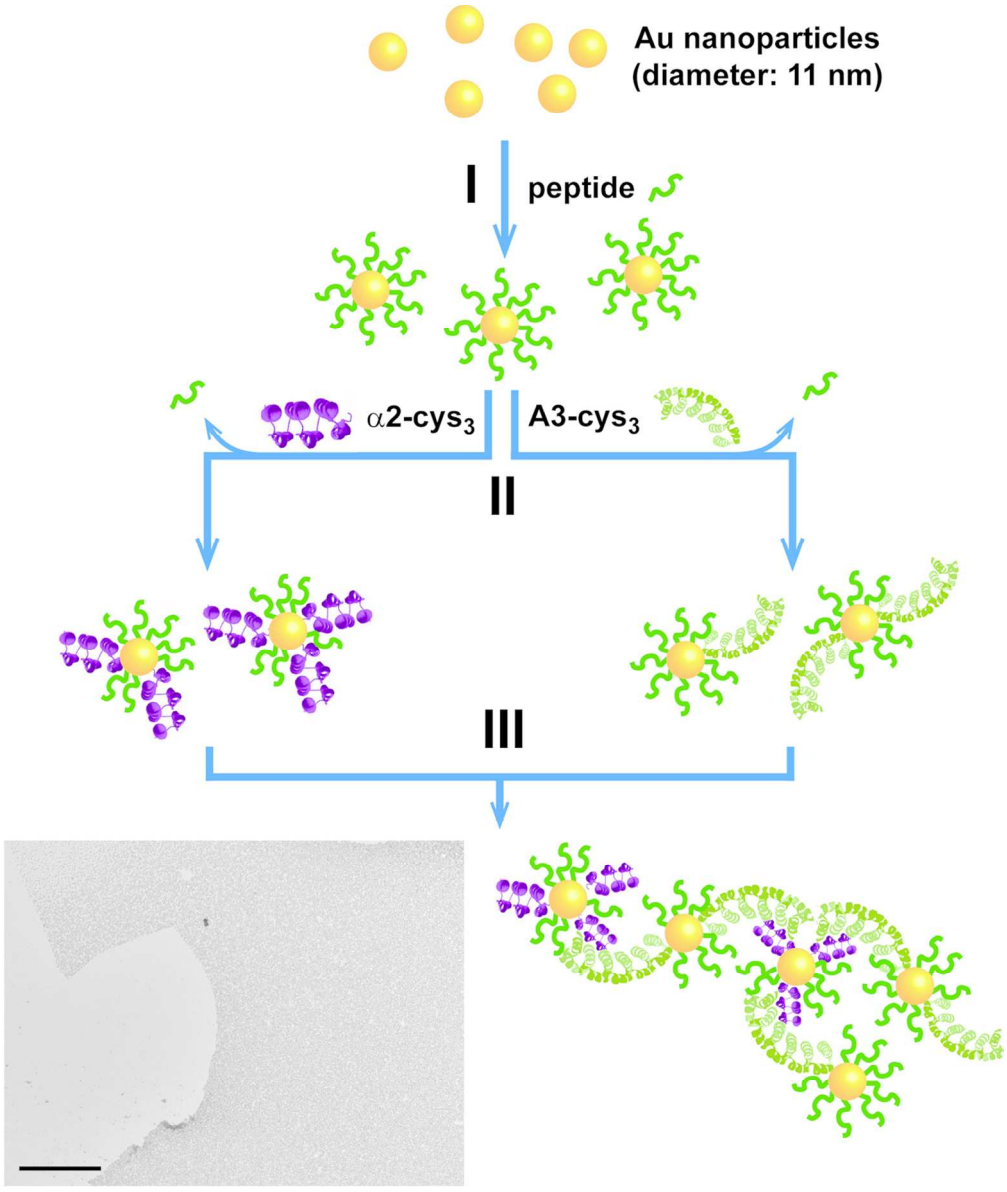
Au nanoparticles
(diameter: 11 nm)
I
peptide
α2-cys3
A3-cys3
II
III

a

(i) MRGSHHHHHHTDPEKVEMYIKNLQDDSYYVRRAAAYALGKI
GDERAVEPLIKALKDEDAWVRRAAADALGQI
GDERAVEPLIKALKDEDGWVRQSAAVALGQI
GDERAVEPLIKALKDEDWFVRIAAAFALGEI
GDERAVEPLIKALKDEDGWVRQSAADALGEI
GGERVRAAMEKLAETGTGFARKVAVNYLETHKSLSCGCGCS

(ii) MRGSHHHHHHTDPEKVEMYIKNLQDDSSVVRKAAAVALGEI
GDERAVEPLIKALKDEDQFVRIAAAWALGKI
GGERVRAAMEKLAETGTGFARKVAVNYLETHKSLSCGCGCS

(iii) MRGSHHHHHHTDPEKVEMYIKNLQDDSWQVRRVVAEALGKI
GDERAVEPLIKALKDEDLAVRRNAALALGKI
GDERAVEPLIKALKDEDPFVRRVAAQALGKI
GGERVRAAMEKLAETGTGFARKVAVNYLETHKSLSCGCGCS

b

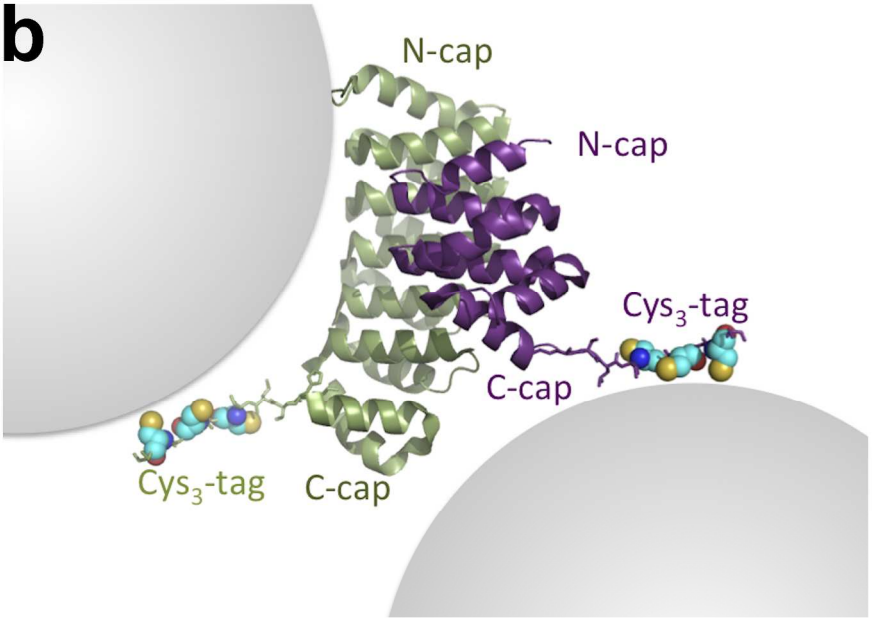

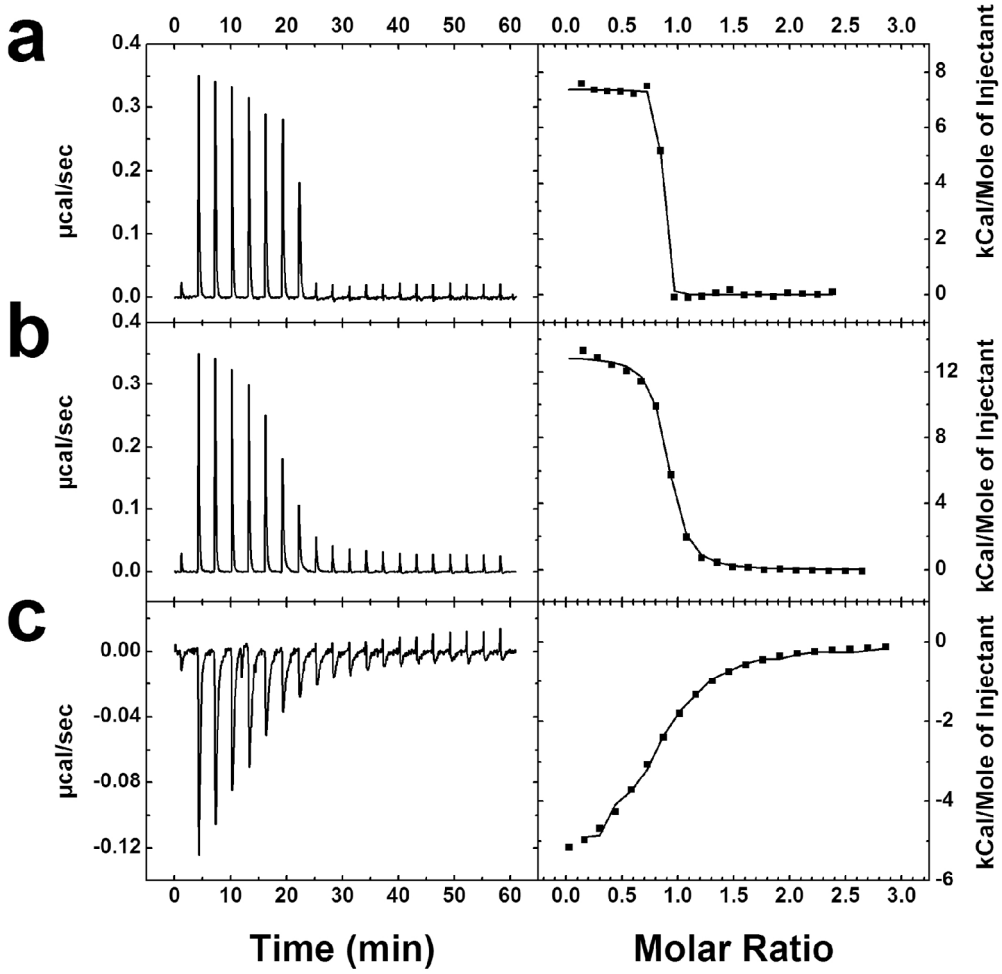

Micro-calorimetry (ITC) analysis of the A3-Cys3-binding activity of (a) α2-Cys3 (30 µM in cell) and (b) α17-Cys3 (30 µM in cell). Experiments performed at 15°C in PBS (50 mM sodium phosphate pH 7, 150 mM NaCl) with 350 µM A3-Cys3 in syringe. For each ITC experiment, the raw data (left panel) is integrated to obtain the saturation curve (right panel). (c) ITC analysis of the competition experiment between 350 µM α2-Cys3 (in syringe) and 25 µM A3-Cys3 pre-bound to 45 µM α17-Cys3 (in cell).

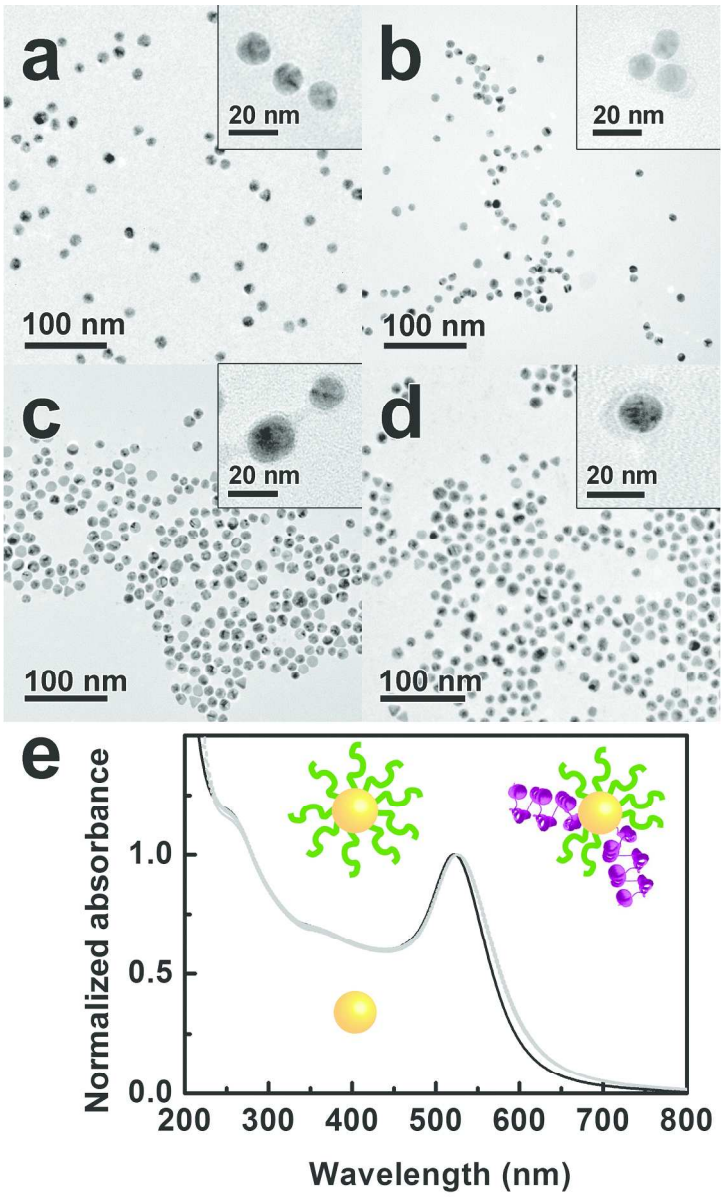

Figure 4. TEM images of (a) Au NPs conjugated with a peptide and exchanged with b) A3cys3, c) α2cys$_3$ and d) α17cys$_3$ proteins. The insets present the TEM images of the corresponding stained samples. (e) Normalized UV-visible spectra of the samples (a) to (d): in black the as-synthesized Au NPs and in grey, the Au NPs functionalized with a peptide or an αRep protein (all data strictly overlap).

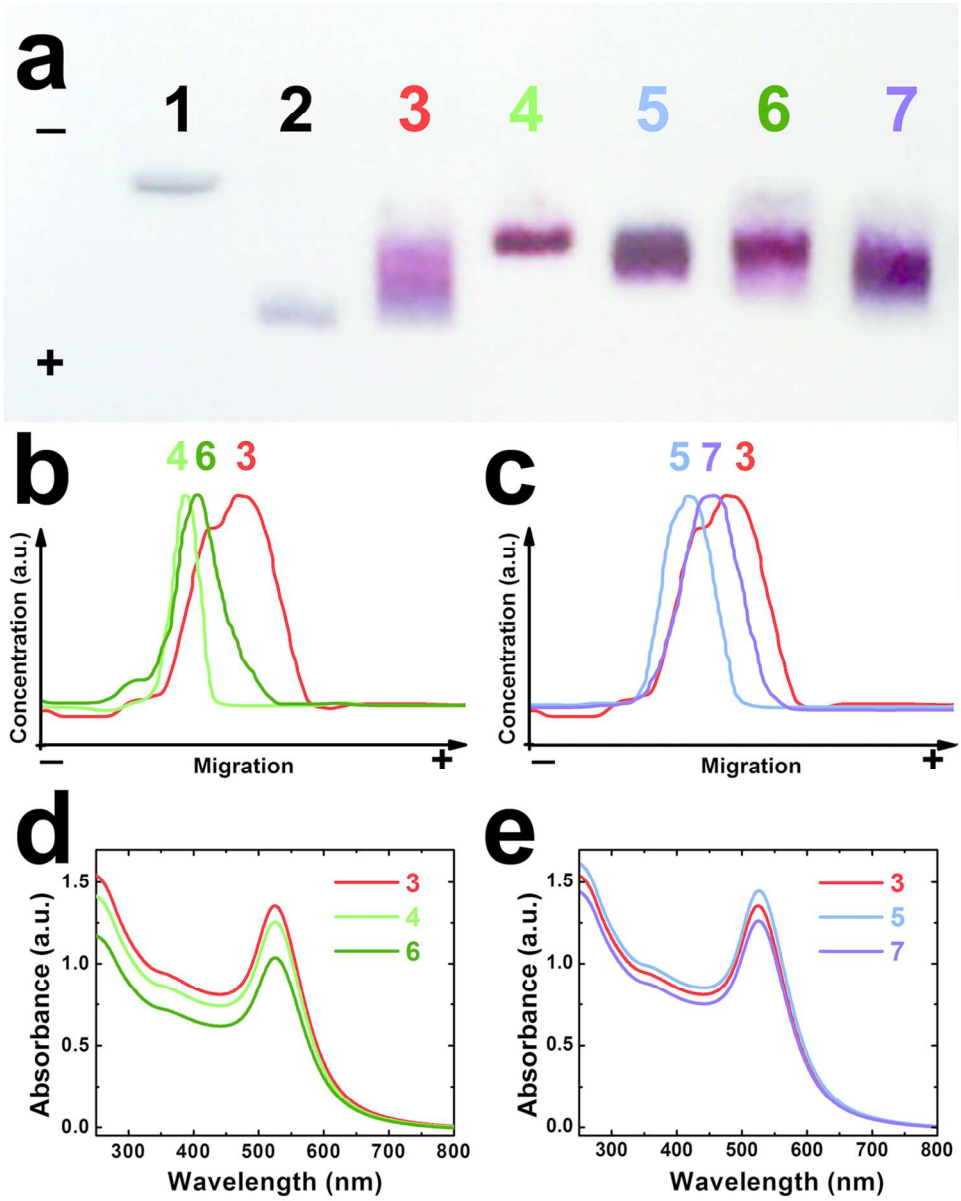

Figure 5. (a) Agarose gel electrophoresis of Au NPs stabilized by (1) citrate or (2) anionic C3E6Asp peptide. Tracks (3) to (5) correspond to Au NPs functionalized with αRep proteins A3-Cys_3, α2-Cys_3 and α17-Cys_3 respectively. The conjugates Au-A3•α2-Au and Au-A3•α17-Au are run in tracks (6) and (7) respectively. (b) Electrophoresis profile plots for tracks (3), (4) and (6) for the self-assembly driven by the A3•α2 pair. (c) Electrophoresis profile plots for tracks (3), (5) and (7) for the self-assembly driven by the A3•α17 pair. (d, e) UV-visible spectrophotometry of the corresponding experiments for (d) the A3•α2 pair and (e) the A3•α17 pair.

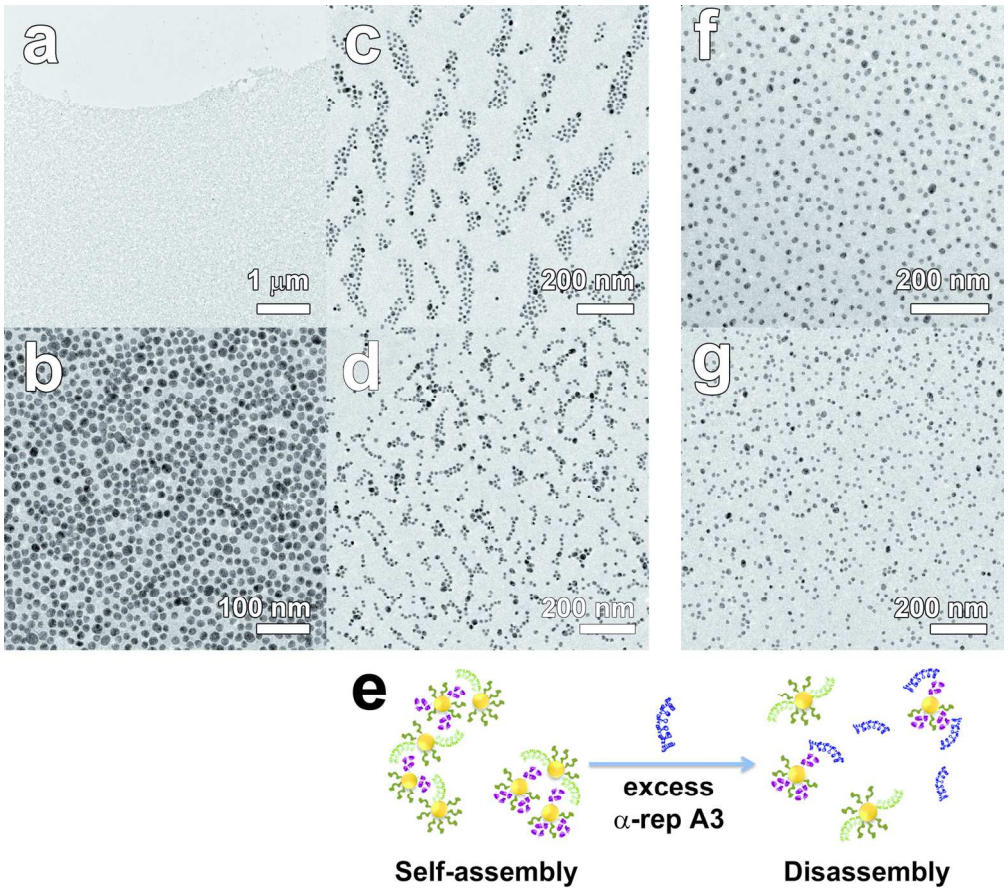

Figure 6. (a-d) TEM images of Au nanoparticles self-assembly induced by the affinity pairing of the conjugates A3•α17 (a, c) or A3•α2 (b, d) at a nanoparticle : protein molar ratio 1 : 30 (a : b) or 1 : 20 (c, d). (e) Schematic of affinity competition tests where the addition of a 10-fold excess of free αRep A3 bearing no cysteine tag induces the disassembly of the nanoparticle conjugates. (f, g) TEM images of the disassembled Au-A3• α2-Au (f) and Au-A3•α17-Au (g) conjugates after incubation in the presence of free A3.

Nanoparticles Self-Assembly Driven by High Affinity Repeat Protein Pairing

Kargal L. Gurunatha[1], Agathe C. Fournier[1], Agathe Urvoas[2], Marie Valerio-Lepiniec[2], Valérie Marchi,[3] Philippe Minard[2] and Erik Dujardin[1]**

[1] Groupe NanoSciences - CEMES-CNRS UPR 8011 - 29 rue J. Marvig, B.P. 94347, F-31055 Toulouse, France. Fax: (+33) 56225 7999. **E-mail: dujardin@cemes.fr**

[2] I2BC, Univ Paris Sud, CNRS, CEA UMR 9198 - Bât. 430, F-91405 Orsay, France. Fax: (+33) 16985 3715. **E-mail: philippe.minard@u-psud.fr**

[3] University Rennes 1, Institut of Chemical Sciences, UMR 6226 CNRS, Campus Beaulieu - F- 35042 Rennes Cedex France

Supplementary Information

1. Materials

Ultra-pure water with a conductivity of 18.2 MΩ/cm was used throughout the experiments. Tetrachloroauric acid ($HAuCl_4$), trisodium citrate ($Na_3C_6H_5O_7$), dithiothreitol ($C_4H_{10}O_2S_2$ - DTT), sodium phosphotungstate dibasic hydrate ($2Na_2O.P_2O_5$ $12WO_3.18H_2O$), boric acid (H_3BO_3), sodium chloride (NaCl) and agarose powder, sodium phosphate (NaP) 50mM pH7 and pH8 buffers were purchased from Sigma-Aldrich and used as received. Negatively charged peptide, Cys-Cys-Cys-21-amino-4,7,10,13,16,19-hexaoxaheneicosanoyl-Asp (C3E6Asp) (>90% purity) was bought from Polypeptide Group and used as received. All glassware was cleaned with aqua regia ($HCl:HNO_3$ 3:1) and rinsed abundantly with ultra-pure water.

2. TEM and UV visible absorption spectrum of citrate-stabilized Au nanoparticles.

The citrate-stabilized Au nanoparticles were synthesized as described in Section 1 of this document and characterized by TEM and UV-visible spectrophotometry as described in Figure S1. The typical average particle diameter was 11 nm with a size distribution of 10-15%. The nanoparticle exhibited a localized plasmon resonance at 520 nm.

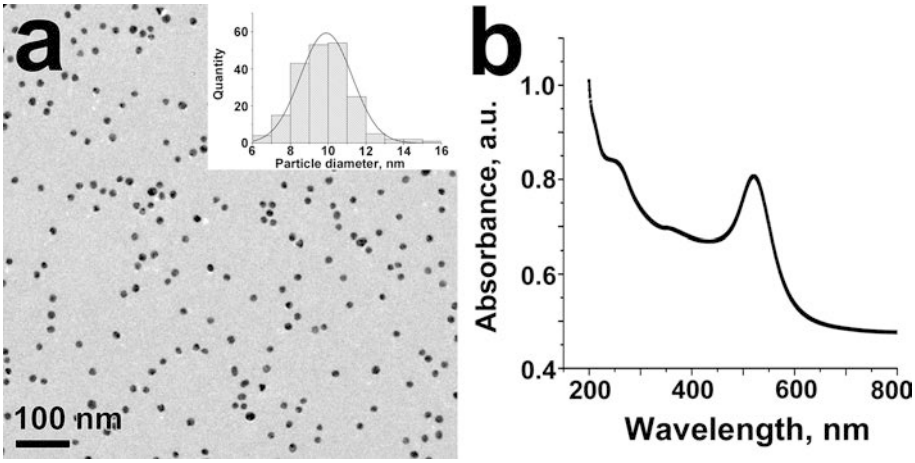

Figure S1. (a) TEM image of citrate-stabilized Au nanoparticles. They are stable and well separated with typical average diameter of 10-11 nm and a standard deviation of 10-15% as illustrated in the inset. (b) UV-visible extinction spectrum.

3. Gel electrophoresis of constituent and assembled protein-functionalized nanoparticles at low colloidal concentration

The protein-driven self-assembly of nanoparticles results from the pairing equilibrium which is affected by the activity of the proteins in solution. As the proteins are immobilized on the surface of the nanoparticles, this activity depends on the nanoparticle concentration.
In Figure S2, the successive synthetic steps leading to protein-functionalized nanoparticles are reproduced by following the protocol described in the main text (Tracks 1 to 5 in Fig. 5). In tracks 6 and 7, the particle suspensions are mixed at low nominal nanoparticle concentration, i.e. without the 5x concentration step described at the end of the protocol.
It can be noticed that the self-assembly does proceed albeit to a much lesser extent, which is observable by the dilute and spread signal in tracks 6 and 7.

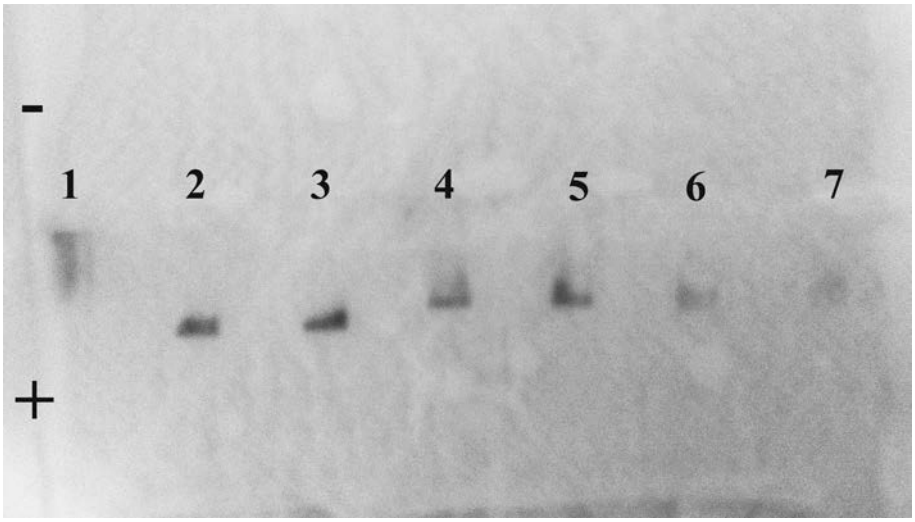

Figure S2. Migration of gold nanoparticle in agarose gel electrophoresis at low nanoparticle concentration. The protocol is identical with the one described in the main text except that the particle suspensions are not concentrated 5 times. Au NPs stabilized by (1) citrate or (2) C3E6Asp peptide. Tracks (3) to (5) correspond to Au NPs functionalized with α-Rep proteins A3, α2 and α17 respectively. The conjugates Au-A3•α2-Au and Au-A3•α17-Au, prepared without the 5x concentration step, are run in tracks (6) and (7) respectively.

4. Spectral shift of the plasmon resonance with the interparticle distance

When Au nanoparticles are brought very close to each other, the localized surface plasmon band (LSP) undergoes a spectral shift towards higher wavelengths because of the dipolar coupling of the LSP borne by the nearest neighbors.[1] This has been widely documented in aggregates of nanoparticles obtained by direct coagulation or by self-assembly driven by small molecules. When, the interparticle gap distance is as small as 1 nm, the spectral shift can be as large as 200 nm.[1, 2]

However, this spectral shift rapidly vanishes as the gap distances increases.
In Figure S3a, the absorption spectra of 11-nm Au nanoparticle dimers placed in a medium of refractive index n=1.5 are calculated as a function of the gap distance of 3, 5 and 7 nm and compared to the one of isolated nanoparticles. A gap distance of 3 nm does produce a distinct redshift but for a gap of more than 5 nm, this shift is almost imperceptible.

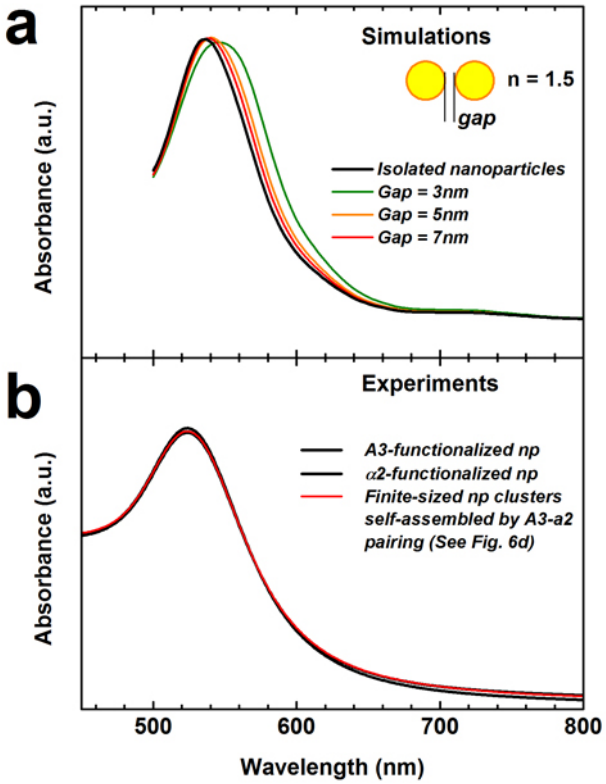

Figure S3. (a) Evolution of the absorption spectra of 11-nm Au nanoparticle dimers as a function of the interparticle gap distance. The refractive index of the surrounding medium is 1.5 (glass). (b) Absorption spectra of isolated nanoparticles functionalized with A3 or a2 proteins (black) and of the self-assembled finite size clusters shown in Fig. 6d (red).

This idealized situation can be compared to the spectra of isolated Au nanoparticles functionalized with complementary proteins (A3, α2 or α17) as described in the main text and the spectra of the self-assembled structure. Figures 6d and 6e present the spectra for the high protein : nanoparticle molar ratio (30 : 1) leading to monolayered films and Fig. S3b shows, for the A3•α2 system, the spectra for the low protein : nanoparticle molar ratio (20 : 1) that is shown to yield finite sized nanoparticle clusters (Fig .6c, d). We observe that the spectral shift upon assembly is imperceptible.
The main reason in the case of the monolayered film (Fig. 5d,e) is that the film settles (or has a small absorption cross-section) and is not probed by spectrophotometry. The spectra (6) and (7) shown in Fig5d-e are due to the nanoparticle NOT assembled in the film but still individually suspended, which thus exhibit a non-shifted maximum. The formation of the film is nevertheless revealed in those

spectra by the decrease in absorption corresponding to the nanoparticles immobilized in the self-assembled film.

For the clusters, which remain in suspension, the absence of shift is consistent with the average gap size that exceeds 5.5 nm (See Section 5 and Fig. S6). We should point out that the simulations in Fig. S3a are done in a glass-like medium of refractive index n = 1.5 in order to increase the redshift, which consequently also redshift the LSP maximum (λ_{max} ~ 535 nm) compared to the aqueous medium of index n = 1.33 used in the experiments of Fig. S3b (λ_{max} ` 520 nm). Moreover, the simulated LSP bands are narrower than the experimental ones because the ohmic losses are slightly underestimated. Consequently, the experimental redshift for a gap size equal or greater than 5 nm is expected to be smaller than the ones obtained in the simulations. Both simulations and experiments are therefore consistent with the fact that protein-pair driven self-assembly, as designed in this work, does not lead to a measurable spectral shift of the LSP.

5. Characterization of freestanding particle film assembled by protein pairing

Web-like filaments that spontaneously form within 48 hours after mixing A3-Au nanoparticles with α2-Au or α17-Au nanoparticles were analyzed by SEM (Fig. S4) and TEM (Fig. S5). For this, droplets containing the filaments were deposited onto a chip of oxidized silicon wafer and left to dry.

Figure S4 shows SEM images taken at several magnifications. Fig. S4a shows that the filaments are made of a uniform, one-particle-thick film that extends overs tens of micrometers. Zoomed in views reveal that the nanoparticles are densely but uniformly packed but no sign of three dimensional stacking or clustering is observed (Fig. S4b). Very occasionally, a second partial monolayer can be observed as in Fig. S4c but it was not possible to attribute such bilayers to self-folded monolayer areas or to areas where self-assembly produced a bilayer region.

The variation in compaction observed in Fig. S4d-f can be attributed to the variation of protein pair crosslinking as the effective concentration increased inside the drying droplet. The structure of the monolayered film in the aqueous medium would thus be similar to the dark areas in Fig. S4d also depicted in Fig. S4f.

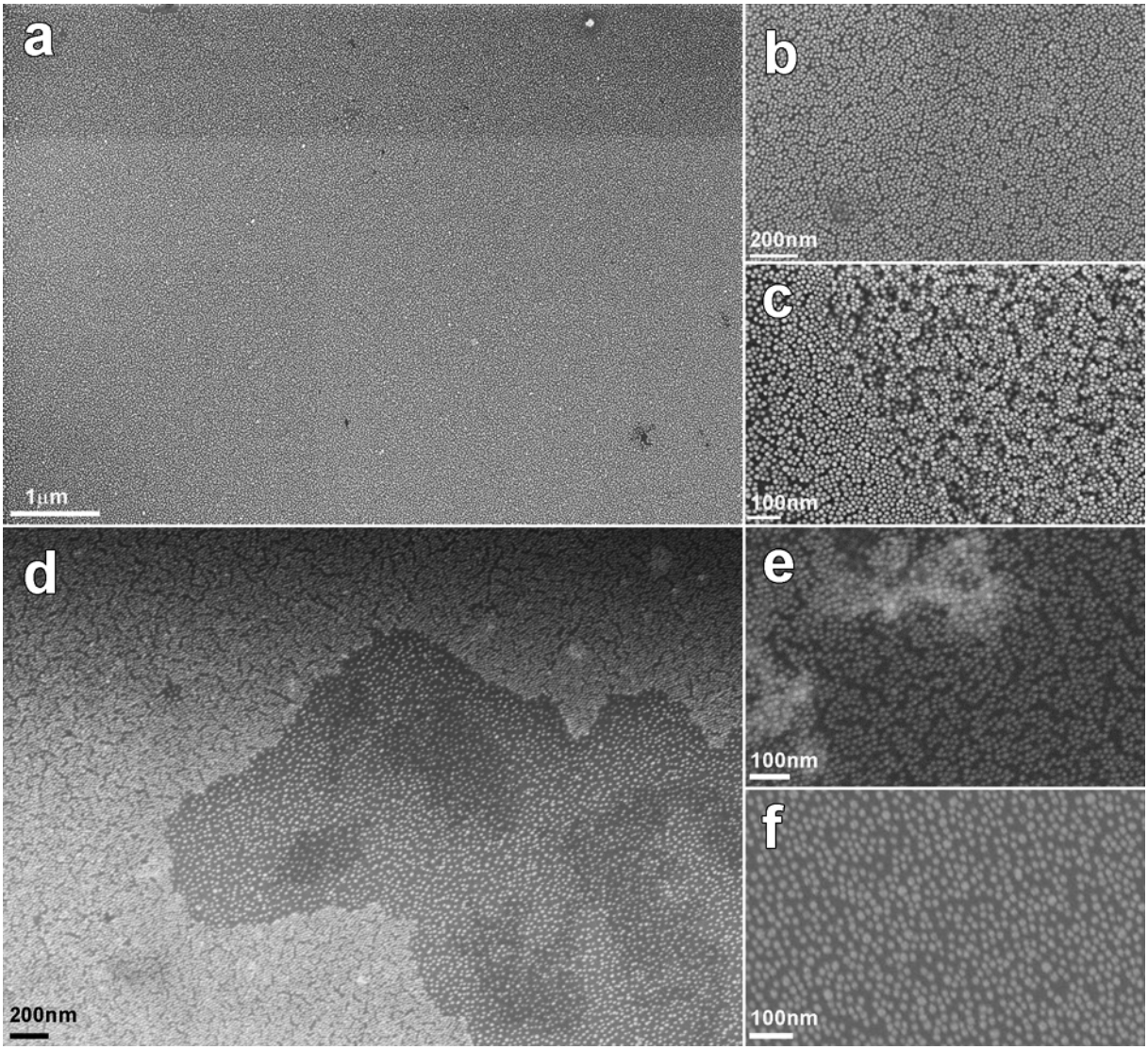

Figure S4. SEM image of Au-A3 conjugate mixed with Au-A17 protein conjugate. (a) Low magnification view of the self-assembled monolayer of Au nanoparticles. (b) Closer view of the monolayer showing the compact arrangement of nanoparticles. (c) Portion of bi-layer found in some rare places. (d) Low magnification view of an area of the monolayer with two levels of compaction. The bright close packed area is magnified in (e) and the more loosely packed zone is magnified in (f).

In complement to Fig. 1 and Fig. 6a in the main text, Figure S5 displays TEM images of free-standing film at low (a-c) and high (d) magnifications. The highly homogeneous monolayered film (including along its edges), the absence of lone clusters and the very few individual nanoparticles in the vicinity of the film edge confirms that the observed film is produced in suspension and not by drying/dewetting on the supporting carbon film. The nanoparticles are surrounded by organic matter with a typical distance to nearest neighbors of about 3-5 nm as seen in Fig. S5d, which is similar to the SEM observations in Fig. S4f.

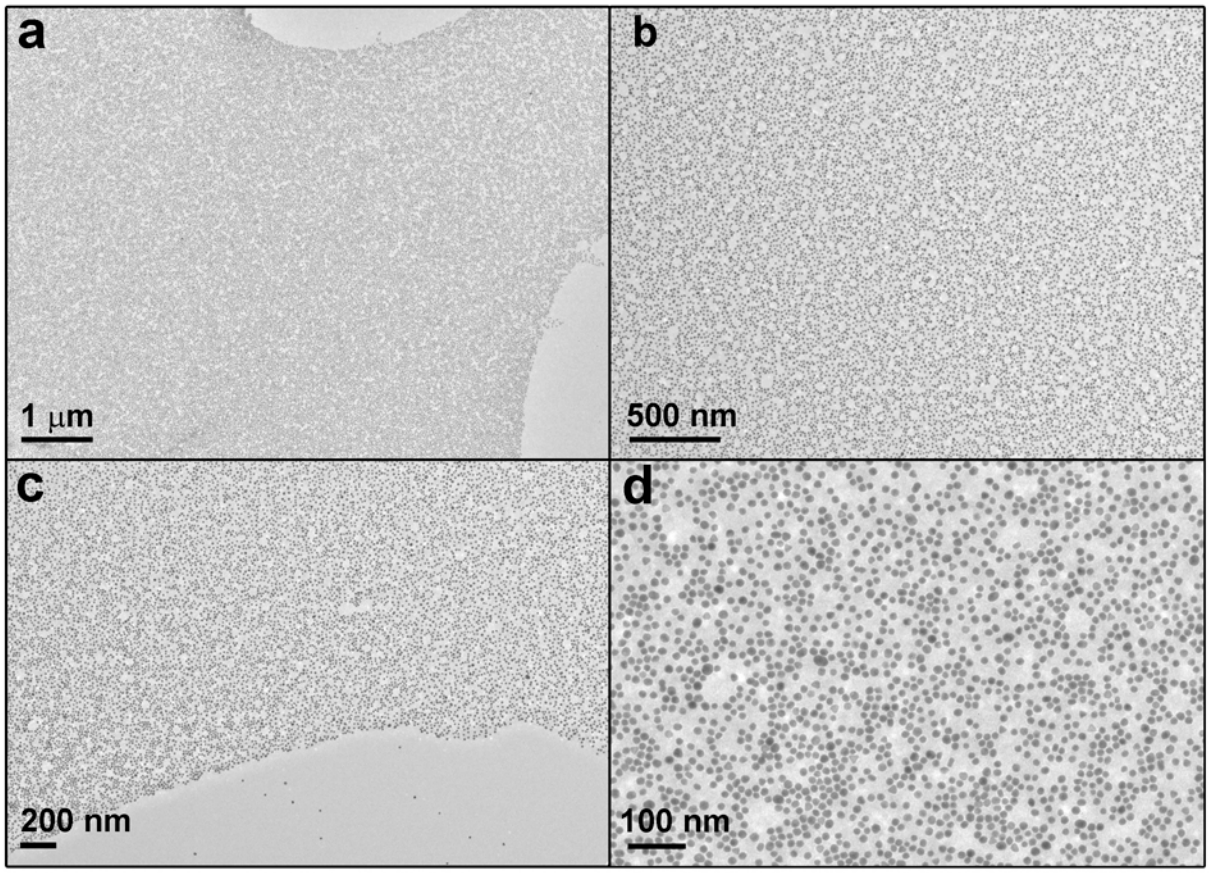

Figure S5. TEM images of Au-A3 conjugate mixed with Au-A17 protein conjugate. (a,b,c) Low magnification views of the self-assembled monolayered film of Au nanoparticles. (d) Closer view of the monolayer showing the compact arrangement of nanoparticles surrounded by organic material.

Within the free standing films constituting the web-like filaments, the Au nanoparticles could be seen as densely and regularly packed with a uniform finite interparticle distance. Figure S6 shows two histograms of the interparticle distance measured from TEM and SEM images. Both distributions coincide on a mean distance of about 3.5 ± 1.2 nm and 4.3 ± 0.7 nm that is in good agreement with the spherical volume of the protein pair of about 5 nm diameter.

A more detailed analysis of SEM and TEM images such as Fig. S4b or Fig. S5b is provided by the 2D auto-correlation analysis of the SEM image in Fig. S6c, shown in Fig. S6d. The auto-correlation shows clear maxima on close-packed sites with intensity maxima along two or three hexagonal rings that indicate a significant correlation with first, second and even third nearest neighbors. The average center-to-center interparticle distance is 17.5 nm, which corresponds to an interparticle gap of about 5.5 nm.

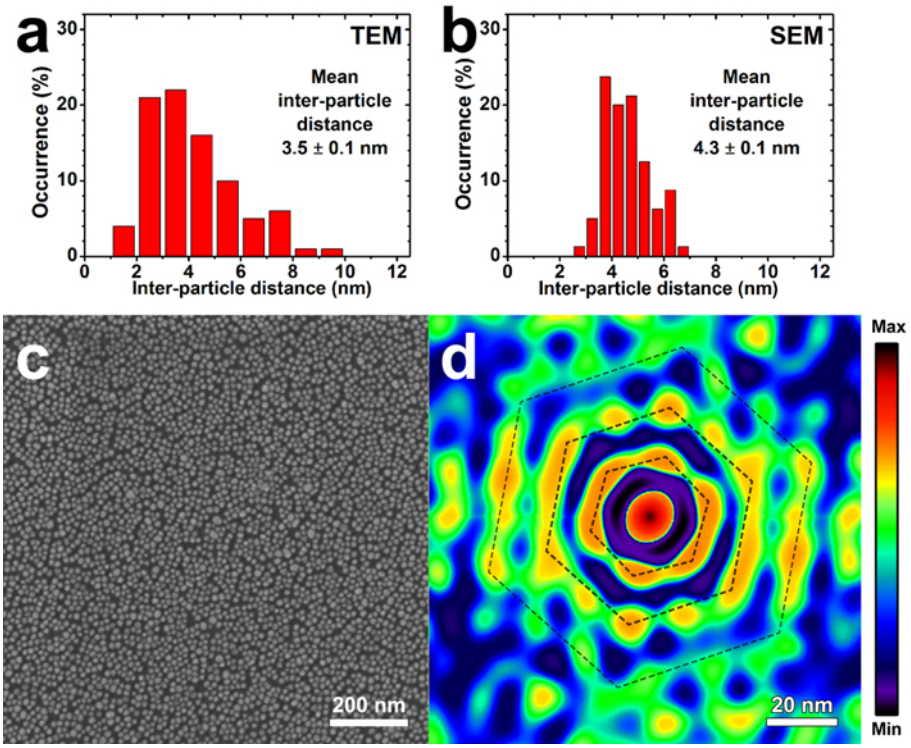

Figure S6. (a, b) Histograms of interparticle distances measured on (a) TEM and (b) SEM images of the nanoparticle filamentous film collected after mixing Au-A3 and Au-α17 conjugates. (c) SEM image and (d) corresponding 2D auto-correlation image showing short range close packed order with first and second nearest neighbors clearly identified by maxima in the auto-correlation function. The third nearest neighbor corona is partially visible too. The center-to-center distance is 17.5 nm corresponding to an interparticle distance of about 5.5 nm.

We note that free-standing nanoparticle films with thickness as small as one nanoparticle have been reported on multiple occasions in the past decade,[8-13] which indicates that 2D assembly is not as unfavorable as it could first appear. While no general mechanism accounts for all systems, which all have specific reasons to undergo 2D assembly, one can distinguish two types of rationale. Nanoparticles with isotropic ability to self-assemble (for example uniformly coated with complementary DNA strands) are confined in 2D spaces by spinning, surface templating, dewetting across small apertures, etc. Alternatively nanoparticles with regioselective and directional assembling interactions can form 2D films in solutions. Anisotropic dipolar interactions, coplanar interacting patches have been shown to yield free-standing films.

In our case, the α-Rep pair formation implies that the concave facet is freely accessible and therefore the proteins (in particular A3) are probably positioned radially to the nanoparticle surface thanks to the Cys_3 linker placed at the C-terminal.

Moreover, owing to their modular structure, the proteins bear a well-defined distribution of charges in the non-variable part of the proteins. In particular, two longitudinal ridges of negative charges are present in the loops bridging the successive double α-helices (sequences DED and DER before and after each helix). When one takes into account the fact that A3 and α17 are rather large (5 nm long) compare to the nanoparticles size (10 nm), it is therefore possible that 3 proteins attached to a given nanoparticle adopt a regular equatorial arrangement.

The rigid protein pair formation evidenced by XRD in our earlier work would preserve the directionality of particle-to-particle attachment through the protein pair.[14] Although this work on the self-assembly of particles decorated with flat interacting patches, which departs from our case where the nanoparticles and the proteins are of similar size, it has shown that nanoparticles with selective directional interactions from equatorial patches leads to stable film formation. Moreover when the

particle bear only two patches with a relative azimuthal angle smaller than 180°, particle rings are formed which are indeed observed in our films (Fig. S5d).

We therefore believe that the combination of low stoichiometry, regular equatorial surface layout of the proteins due to the inter-protein charge interactions and steric hindrance along with rigid protein pair formation contribute to favor coplanar assembly of the nanoparticles.

6. Link between protein : nanoparticle stoichiometry and self-assembly topology

The grafting of the a-Rep proteins onto the nanoparticles is obtained through thiol-Au bond formation, which is quantitative, the surface chemistry is not limiting and more than one protein can definitely be attached to the nanoparticles. Yet their maximum number is rather limited owing the comparable size of the proteins (A3, and α17) with the nanoparticles and the significant charge borne by them at pH7. If the nanoparticles were covered with more than 4 proteins, reticulated and isotropic 3-dimensional aggregation would occur which was not seen for the finite sized aggregates nor alongside the extended film formation. This observation indicates that the stoichiometry remains essentially between 1:1 and 3:1 protein per particle.
In Figure 5, the breadth of the GEP bands No3 and 5 indicates that we have a range of stoichiometry for the high feeding ratio. The corresponding GEP bands No3 and 5 obtained for the low feeding ratio (Fig. S2) are both narrower and relatively closer to the injection well. This observation is consistent with a smaller number of proteins attached, on average, on the nanoparticles and the stated observation that a higher feeding ratio leads to larger aggregates (film) and a smaller feeding ratio to finite sized clusters. A similar interpretation of α2 is less straightforward since this protein is much smaller and the variation of stoichiometry does not affect significantly the charge / size of the bioconjugate.

When nanoparticles bear 1, 2, 3 or more proteins able to bind complementary partners, the topology of the resulting self-assembly structure will depend on the relative amount of each types of nanoparticles, as illustrated in Figure S7.

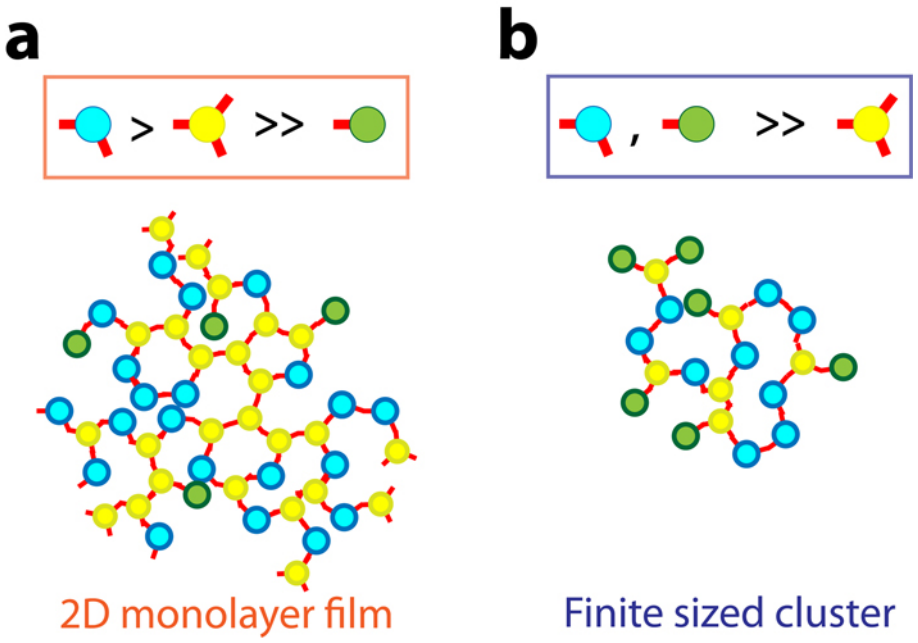

Figure S7 Schematics of some topologies adopted by self-assembled nanoparticles superstructures when relative amount of particles bearing 1, 2 or 3 binding proteins is modified. (a) When nanoparticles bearing a single proteins are much less numerous than ones bearing 2 or 3 proteins, the network can expand largely. If ditopic particle prevail, the 3-dimnesional branching is limited and the resulting self-assembly can be restricted to monolayered films. (b) If particles bearing 3 proteins are present but in small amount, the di- and monotopic particles will rapidly limit the growth extension and finite sized clusters are formed.

With pure 1:1 stoichiometry, i.e. nanoparticles bearing a single protein, only dimeric structure can be produced.

With a mixture or mono- and ditopic (2:1 stoichiometry) particles, chains will be formed, the length of which will vary with the relative amount of mono- vs ditopic particles.
As soon as tri-topic particles (3:1 stoichiometry) are introduced, the self-assembled structures can expand as a 3D network, which will grow all the more that monotopic particles are scarce and unable to stop the nanoparticle concatenation. Yet, the relative amount or di- vs tritopic particles may favor the formation of 2D assembly. In particular if tri-topic nanoparticles are significantly less frequent than ditopic ones (Fig. S7a), the potential for 3D networking is limited and the self-assembly can proceed in 2D resulting in monolayered film as observed in this work and earlier reports for semiconductive nanoparticles (Kotov et al., *Science* **2006**, 314, 274-278) and for DNA-linked metal nanoparticles (D. Luo et al, *Nature Materials*, **2009**, 8, 519-25), for example.
If the number of available proteins is further reduced, leading to few tri-topic particles but mostly di- and monotopic particles, the expansion of the self-assembly is limited by the incorporation of mono-topic particles that stop the chain growth, thus quickly stopping the development of the aggregates. This results in finite sized clusters as illustrated in Fig. S7b and experimentally observed in our case in Figs. 6c and 6d.

7. References

1. Dujardin, E.; Girard, C. Plasmonic Nanoparticle Networks. In *Handbook of Nanophysics* Sattler, K., Ed. Taylor & Francis: London, 2010; Vol. 3.
2. Lin, S.; Li, M.; Dujardin, E.; Girard, C.; Mann, S. One-Dimensional Plasmon Coupling by Facile Self-Assembly of Gold Nanoparticles into Branched Chain Networks. *Adv. Mater.* 2005, 17, 2553-2559.